

Factors affecting the performance of a low-pressure submerged membrane photocatalytic reactor

Sze Sze Chin^a, Tuti Mariana Lim^{a,b}, Ken Chiang^c, Anthony Gordon Fane^{a,*}

^a School of Civil and Environmental Engineering, Nanyang Technological University, Block N1, Nanyang Avenue, Singapore-639798, Singapore

^b Institute of Environmental Science and Engineering, Innovation Centre, Block 2, Unit 237, 18 Nanyang Drive, Singapore-637723, Singapore

^c ARC Centre for Functional Nanomaterials, School of Chemical Engineering and Industrial Chemistry, The University of New South Wales, Sydney, NSW 2052, Australia

Abstract

A hybrid system combining a low-pressure submerged membrane module and a photocatalyst suspension was used to purify water containing bisphenol-A (BPA). The influences of pH, aeration rate, titanium dioxide (TiO₂) and initial BPA concentration were investigated in batch kinetic tests. In these studies, a combination of pH 4, 0.5 g/L TiO₂ and 0.5 L/min aeration rate were determined to be the optimized conditions for application in the continuous submerged membrane photocatalytic reactor (SMPR). The effect of initial BPA concentration in the range of 5–50 ppm fits the Langmuir–Hinshelwood (L–H) kinetics well. With 100 L/(m² h) of permeate flux which resulted in 2 h residence time, 97% degradation and higher than 90% mineralization of the 10 ppm BPA were achieved after 90 and 120 min, respectively. The effect of filtration flux and intermittent permeation were also studied in terms of production rate of treated water, efficiency of the SMPR and membrane performance sustainability. A simple CSTR model had limited success predicting the effect of initial concentration of BPA on the performance of the SMPR. The SMPR has the potential to be used for removing low concentrations of organic pollutants in a more cost effective way.

© 2006 Published by Elsevier B.V.

Keywords: Aeration; Low-pressure; Submerged membrane; Photocatalysis; TiO₂

1. Introduction

Titanium dioxide (TiO₂) photocatalysis has become a very active field of research [1–3]. When incident photons of a wavelength less than 385 nm are absorbed by TiO₂, electrons are promoted from the valence band to the conduction band. This excitation brings electrons to the conduction band and leaves positive holes in the valence band. The holes are strongly oxidizing and are capable of oxidizing many adsorbed organics and/or to produce hydroxyl radicals from adsorbed water molecules for further oxidation reactions. However, these charge carriers may also recombine thus reducing the overall efficiency of the photocatalytic process.

Although TiO₂ is known to be a good photocatalyst in terms of its photoactivity, physical and chemical stability, the recovery of the sub-micron sized photocatalysts remains the main engineering concern for large-scale applications. Immobilizing

particulate TiO₂ on a substrate could eliminate the need for particle recovery, however, catalyst immobilization usually impedes mass transport [2]. For the suspended photocatalyst system, several attempts have been made to facilitate the recovery of particulate catalysts which include improving the aggregation of TiO₂ through pH adjustment [4] and enhancing the separation of TiO₂ in a magnetic field by coating it onto magnetic particles [5]. These methods enhance sedimentation and thus facilitate the recovery of the catalysts in a batch process. Nevertheless, a limitation to these methods is that the treated water cannot be withdrawn continuously during the oxidation process without losing any TiO₂ catalysts.

Membrane technology could improve the implementation of the photocatalytic oxidation (PCO) process by enhancing the separation of particulate TiO₂ from the treated water. In this case, a higher throughput of treated water may be achieved. Molinari et al. [6,7] and Sun et al. [8] have attempted to combine photocatalysis and membrane technologies into a single module. Molinari et al. [6] demonstrated the degradation of humic acid, organic dyes and 4-nitrophenol using a hybrid photocatalytic–nanofiltration unit operating at a system pressure

* Corresponding author. Tel.: +65 67943801; fax: +65 6792 1291.
E-mail address: agfane@ntu.edu.sg (A.G. Fane).

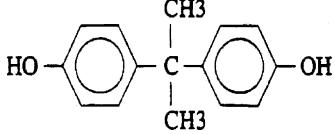
of 6 bar. In their study, the use of nanofiltration (NF) membrane was to retain both the photocatalysts and the organics in the system during the photocatalytic reaction. However, smaller molecular size intermediates that formed during the photocatalytic process were still able to pass through the nanofiltration membrane, which lowered the overall efficiency. Sun et al. [8] reported the deactivation of *Escherichia coliform* (*E. coli*) by using a combination of an inorganic-based ceramic membrane and a composite $\text{TiO}_2\text{-Fe}_2\text{O}_3$ photocatalyst. Their results showed that deactivation of the *E. coli* was as high as 99%.

The membrane options for use with photocatalytic reaction include high-pressure NF as used by Molinari et al. [6], or low-pressure membranes such as micro- and ultrafiltration (MF and UF). NF has the advantage of retaining low molecular weight species but the low-pressure MF and UF have an energy benefit over NF and can be used as submerged membranes. Submerged membranes are now widely used in membrane bioreactors (MBR) owing to the recognized advantages of lower cost of fabrication and maintenance [9,10]. The key features of the submerged membrane module include air bubbling as the main mechanical method to provide membrane cleaning action and suction to withdraw the permeate from the system to prevent overpressure of the reactor. The non-pressurized open system also reduces the overall operating cost of the submerged membrane system. Fu et al. [11] have described a submerged membrane photocatalytic reactor (SMPR) for the degradation of fulvic acid. The reactor consisted of two compartments for filtration and photocatalytic oxidation. An 'in-house' synthesized TiO_2 was used and was reported to enhance separation of TiO_2 and to maintain high flux of filtrate due to the larger particle size compared to Degussa P25. It was also shown that a removal of 73% of total organic carbon (TOC) was achieved within 2 h of UV irradiation.

To the best of our knowledge, the study of SMPR for water purification is limited. Hence, the objective of this paper is to investigate the influence of different operating parameters on the removal of a trace organic, bisphenol-A (BPA) in a SMPR. The SMPR used in this study consisted of a low-pressure submerged hollow fibre membrane module which was in direct contact with the photocatalytic oxidation medium. Selection of membrane

Table 1
Bisphenol-A characteristics

Chemical name	Bisphenol-A (BPA)
Molecular formula	$\text{C}_{15}\text{H}_{16}\text{O}_2$
Molecular weights (g/mol)	228
Solubility at 22 °C (mg/L)	120–300
Vapour pressure at 25 °C (mmHg)	<1
Density at 22 °C (g/cm^3)	1.195

Chemical structure	
--------------------	---

material based on our previous work allowed the integration of the membrane module and the photoreactor [12]. The effects of pH, concentration of TiO_2 and aeration rate were first investigated in a separate batch photocatalytic reactor in order to determine the optimum degradation conditions. The optimized conditions were then used in a continuous SMPR to study the effects of initial BPA concentration and filtration flux. The possibility of using intermittent permeation to control fouling of the membrane was also investigated.

2. Experimental

2.1. Materials and analytical measurements

The P25 TiO_2 used for the experiments was supplied by Degussa AG, Germany. High purity BPA (Merck-Schuchardt) was used and the physical and chemical characteristics of BPA are shown in Table 1. The pH of all suspensions was adjusted using sodium hydroxide and perchloric acid. Purified air was used as a source of oxygen in this study. Unless otherwise stated, all solutions were prepared using Millipore MilliQ (MQ) water with a resistivity of 18.2 $\text{M}\Omega\text{ cm}$. The microfiltration membranes made of polyvinylidene fluoride (PVDF) were supplied by Bluestar China, with an average pore size of 0.2 μm and outer diameter of 1 mm. The choice of PVDF membranes was based on our previous studies [12].

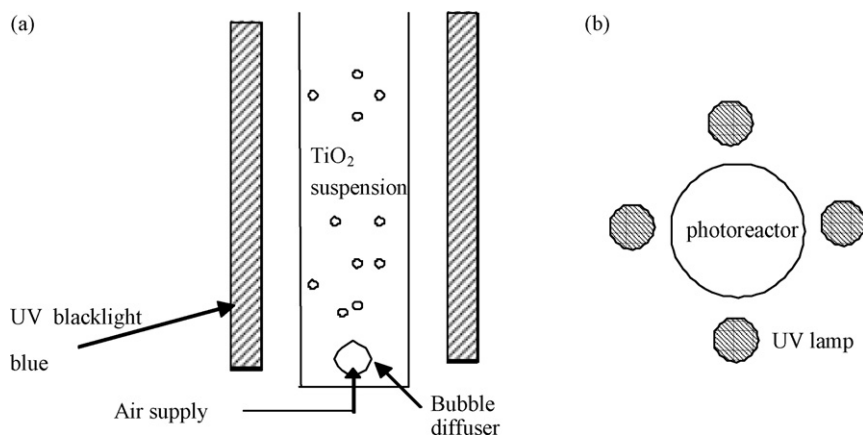


Fig. 1. Schematic diagram of the batch photoreactor experimental setup.

2.2. Batch photocatalytic reactor

Batch photocatalytic tests were carried out in a photoreactor made of borosilicate glass (Fig. 1). UV-A irradiation was provided by four 8 W black light fluorescent lamps (NEC FL8 BL-B) located on the four sides of the photoreactor. The lamps used had an emission of wavelengths from 300 to 420 nm with a peak at 355 nm. An 800 mL of TiO₂ suspension was prepared by adding pre-determined amounts of TiO₂ and BPA followed by pH adjustment using perchloric acid and sodium hydroxide. The concentration of TiO₂ was varied from 0.2 to 2 g/L and the concentration effect was studied at three different pH values of 4, 7 and 10. The final solution, containing 10 ppm BPA, was sonicated for 10 min before charging into the photoreactor. In all experiments, the initial concentration of BPA was kept at 10 ppm unless otherwise stated. The air bubbling in the system was supplied by a purified air cylinder and distributed through a ceramic bubble diffuser. The effect of aeration rate was studied in the range of 0.2–5 L/min (superficial gas velocities of 2.9×10^{-4} to 5.9×10^{-4} m/s). For the study of bubble cloud effects, one of the 8 W UV-BLB lamps was switched on. The incident light intensity, with or without aeration, was then measured using a radiometer (International Light PMA 2200) with an UV-A sensor (PMA 2110) at the wall of the photoreactor (opposite to the lighted lamp). In this way, light transmission through the MQ water in the 65 mm diameter photoreactor was measured. Samples at predefined time were taken, filtered through 0.22 μm filters and analyzed accordingly with different techniques (see Section 2.5). The TiO₂ particle size distributions at different aeration rates were measured at the end of each experiment.

2.3. Submerged membrane-photocatalytic reactor

The schematic diagram of the submerged hollow fibre micro-filtration system is shown in Fig. 2. It consists of a borosilicate

glass photoreactor, similar to the one used in the batch kinetic tests, together with a portable hollow fibre membrane module having an effective area of 4.1×10^{-3} m² placed in the centre. It should be noted that in this system, the membrane module was submerged in the reactor and not in a separate chamber, unlike Fu et al. [11]. This approach should provide a more compact system, but requires careful selection of membrane material [12] as noted earlier. During the experiments, a constant flux of 100 L/(m² h) permeate was withdrawn from the system through the suction provided by a peristaltic pump. The transmembrane pressure (TMP) in all experiments was measured by an online pressure gauge on the permeate line. A level sensor was used to control the feed rate of 10 ppm BPA solution to the system in order to keep the total volume of the reactor constant. Samples at predefined times were taken from the permeate line and analyzed for BPA and total organic carbon concentrations. The effect of permeate flux (40, 60 and 100 L/(m² h)) on the degradation of 20 ppm of BPA solution was conducted by changing the permeate pump settings accordingly. The effect of different constant feed concentration of BPA at 10, 20 and 50 ppm was also studied.

2.4. Membrane adsorption and residence time distribution (RTD) tracer tests

The determination of membrane adsorption was performed using a pulse input tracer test in the SMPR reactor as shown in Fig. 2, with or without the membrane module. Initially, MQ water was continuously drawn through the membrane module before a certain amount of BPA was injected to the reactor as a pulse input. The injected BPA was immediately mixed in the system by the 0.5 L/min of bubbling provided. After the introduction of the BPA, the inlet of the MQ water to the system was stopped so that the concentration of the BPA in the system was fixed at 10 ppm after the dilution of the injection.

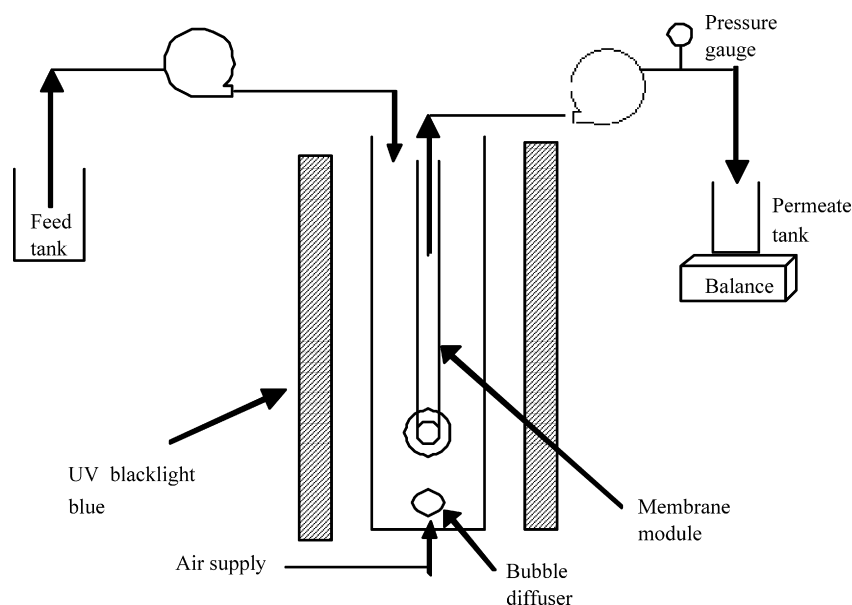


Fig. 2. Schematic diagram of the continuous submerged membrane photoreactor experimental setup.

The corresponding BPA concentration was then taken from the tank and at the permeate line after a predetermined time. For the determination of the residence time distribution of the SMPR system, a sodium chloride tracer test was performed and the procedure was similar to the above except that the MQ water was continuously sent to the system after injection of the sodium chloride. Sodium chloride instead of BPA was used in the RTD test in order to avoid membrane adsorption issue.

2.5. Analytical methods

The concentration of BPA in samples was measured using a high performance liquid chromatograph (Waters Alliance) interfaced with a photodiode array detector. The separation was carried out by a Waters Xterra RP18 HPLC column (3.9 mm × 150 mm, 5 μm) with a mobile phase consisting of 50% water and 50% acetonitrile. The TOC present in the samples was determined by a TOC analyzer (Shimadzu TOC-V_{CSH}). The concentration of sodium chloride was determined using ion chromatography (Shimadzu LC-10Ai). The particle size distribution and turbidity of samples were measured by a Brookhaven ZetaPals particle sizer and a HACH 2100AN IS turbidity meter, respectively. The TOC contributed by the BPA was calculated using Eq. (1).

$$\text{TOC}_{\text{BPA}} = \left(\frac{\text{Number of carbon} \times M_r \text{ Carbon}}{M_r \text{ BPA}} \right) \times C_o \quad (1)$$

where M_r is the molecular weight and C_o is the initial concentration of organics used in the experiment.

3. Results and discussion

3.1. Batch photocatalytic reactor

3.1.1. Influence of initial pH

The initial degradation rates obtained at different pH are shown in Table 2. As observed, the degradation rate at pH 4 was about two times the rate at pH 10. Acidic conditions favour the degradation of BPA and this finding agrees with those reported by Watanabe et al. [13] and Chiang et al. [14]. The point of zero charge (pzc) of Degussa P25 TiO₂ particles is around pH 6.3, hence the TiO₂ surface should be positively charged under acidic media. From the simulation of molecular point charges of all the non-hydrogen atoms in BPA, it is found to possess two negative oxygen atoms at the hydroxyl groups and four negative carbon atoms ortho to the phenolic group [13]. It is thus expected

Table 2

The rate of degradation of 10 ppm of BPA under different pH conditions (TiO₂ concentration = 0.5 g/L, initial BPA concentration = 10 ppm, aeration rate = 1 L/min)

pH	Initial degradation of BPA (mg/(L min))
pH 4	0.225
pH 7	0.187
pH 10	0.124

Table 3

The rate of degradation of 10 ppm of BPA under different TiO₂ concentration conditions (initial BPA concentration = 10 ppm, pH unadjusted, aeration rate = 1 L/min)

TiO ₂ concentration (g/L)	Initial degradation of BPA (mg/(L min))
0.2	0.220
0.5	0.264
1.0	0.235
2.0	0.240

that attractive forces are developed between the substrate and the TiO₂ surface, resulting in high adsorption in acidic medium. The rapid adsorption is expected to enhance the degradation of BPA since photocatalytic oxidation is a surface-oriented reaction. As the pH increases, the TiO₂ surface becomes progressively more negative which leads to the development of greater repulsive forces between the TiO₂ surface and the adsorbate, and therefore retardation of degradation of BPA.

3.1.2. Influence of TiO₂ concentration

In the present study, it was found that the optimum TiO₂ concentration to be used for the degradation of 10 ppm of BPA was 0.5 g/L (Table 3). 0.2 g/L of TiO₂ resulted in the slowest reaction rate and this may be due to the fact that there were lesser active sites available for the adsorption and degradation of BPA. Beyond 0.5 g/L, adverse effects on the degradation rate of BPA can be observed. Although the total surface area available for reaction was higher in the 2 g/L test compared to the 0.5 g/L test, the initial reaction rate was found to be lower (0.240 mg/(L min) compared to 0.264 mg/(L min)). The decrease in efficiency might be attributed to light scattering of UV light by the TiO₂ particles themselves [15].

3.1.3. Influence of aeration rate

Aeration is important for both the separation process by submerged membranes and the oxidation reaction in photocatalytic processes. The former process requires mechanical agitation from aeration in order to reduce the fouling of the membrane surface as well as to keep the TiO₂ well-suspended in the solution; whereas, the latter process requires dissolved oxygen to act as an oxidant and to slow down the electron–hole recombination reaction. Fig. 3 shows that the initial photodegradation rate increased with increasing bubbling rate and reached a maximum value at a bubbling rate of 0.5 L/min beyond which a slight decrease in the degradation rate was observed. Taking a further look at the inset in Fig. 3, it can be seen that though 0.5, 1 and 4 L/min had different initial degradation rates, all tests removed BPA completely by 60 min of illumination time. This trend of results was reproducible. Lee et al. [16] who performed their experiment in a fluidized photocatalytic reactor reported a similar observation. In their experiment, bubbling enhanced the photodestruction of Methyl Orange and its effect reached a plateau above 2 L/min.

In a bubbling system, aeration can affect the size of catalyst aggregates. The effect of aeration on the size distribution

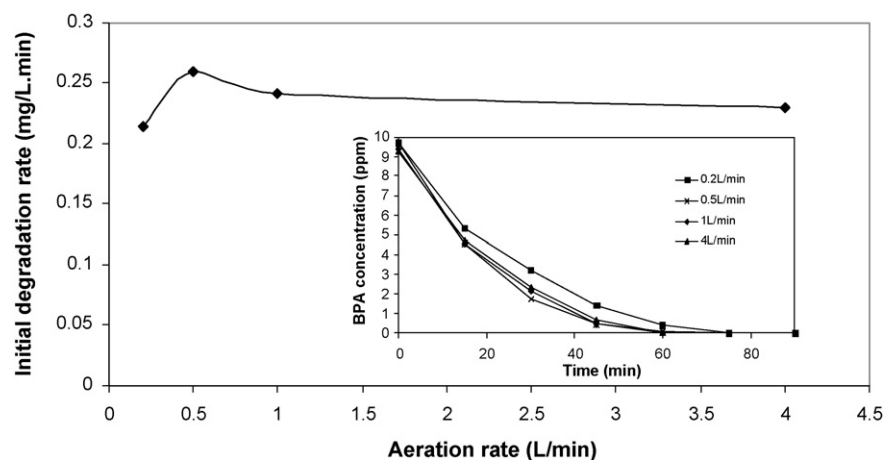


Fig. 3. Photodegradation of BPA as function of different aeration rate (TiO_2 concentration = 0.5 g/L, initial pH 4, initial BPA concentration = 10 ppm).

Table 4

Average particle size of TiO_2 at different aeration rate (initial pH 4, TiO_2 concentration = 0.5 g/L)

Aeration rate (L/min)	Mean particle size (nm)
0.2	757 ± 147
0.5	477 ± 49
1.0	491 ± 52
4.0	309 ± 32

Table 5

Intensity of light measured with different bubbling rate

Aeration rate (L/min)	Light intensity (mW/cm^2)
No bubbling	1.22
0.2	1.20
0.5	1.08
1.0	0.89
4.0	0.60

of the TiO_2 particles is shown in Table 4. It can be seen that after 1.5 h of aeration at 0.2 and 4 L/min, the average diameters (d_{50}) of TiO_2 were found to be 0.75 ± 0.15 and 0.31 ± 0.03 μm , respectively. Higher aeration rates produced greater shear rates which disintegrated aggregated particles. Additionally, with lesser agglomeration occurring, a higher surface area on the smaller particles might be available for the degradation of BPA. This explains why 0.2 L/min resulted in the slowest degradation rate as observed in Fig. 3. Similar negative effect of TiO_2 particles agglomeration on the photocatalytic activity was also reported by Soparajee et al. [17].

Increasing bubbling not only resulted in smaller particles as discussed before, but can also increase the liquid film mass transfer coefficient around the aggregates [18]. It should then

be expected that increasing bubbling rate will increase the photodegradation rate. However, in our system, no enhancement of photodegradation rate was observed beyond 0.5 L/min. This was probably due to the presence of bubble clouds that could attenuate UV light transmission in the photoreactor. As illustrated in Fig. 4, dense bubble clouds were formed during 4 L/min bubbling. The light intensity through the 65 mm diameter photoreactor was measured and found to decrease as bubbling rate increased (Table 5). Light intensity at 4 L/min was only 55% of that at 0.5 L/min. Though this measurement does not show the absolute value of the light intensity in the system, it confirms the idea of possible light attenuation by bubble clouds. Thus, this may explain the plateau observed as aeration increases. The possibility of bubbles ability to scatter light was also studied

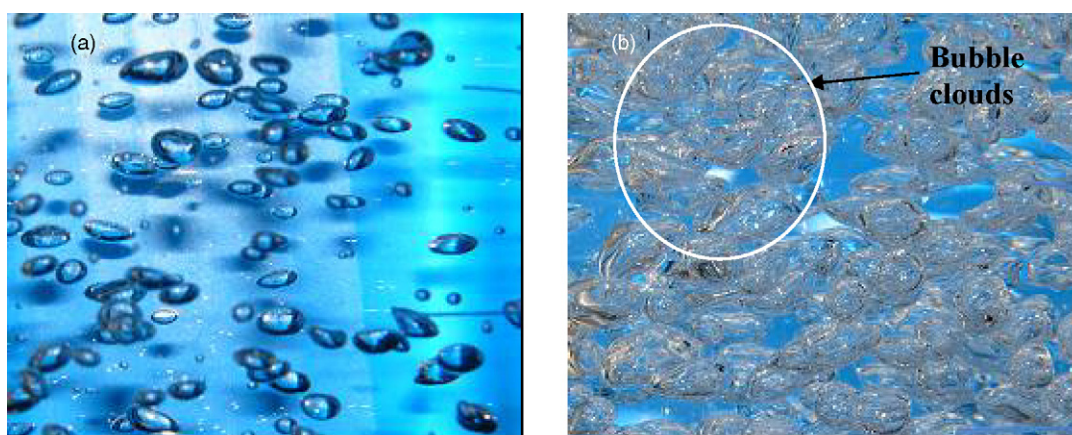


Fig. 4. Bubbles resulted from: (a) 0.5 L/min and (b) 4 L/min of aeration rate.

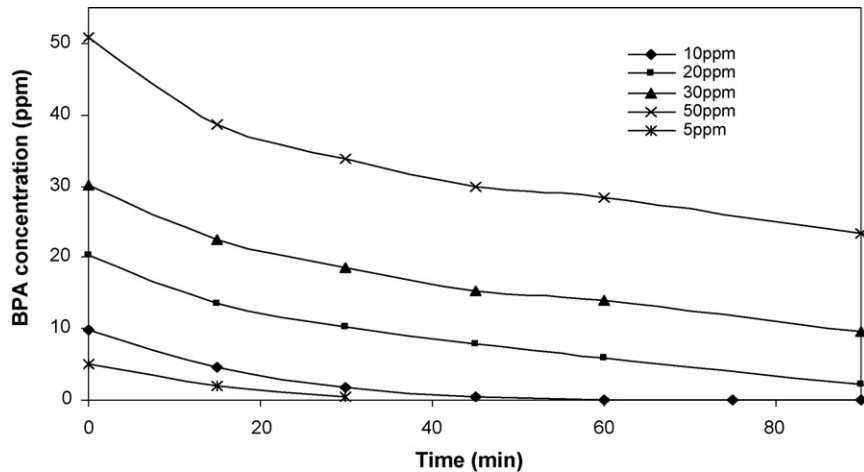


Fig. 5. Influence of initial concentration of BPA (TiO_2 concentration = 0.5 g/L, initial pH 4, BPA feed concentration = 10 ppm, 0.5 L/min aeration rate).

Table 6

Reaction rate constant for different initial concentration of BPA (TiO_2 concentration = 0.5 g/L, initial pH 4, aeration rate = 0.5 L/min)

Initial concentration of BPA	k (min^{-1})
10	0.0569
20	0.0223
30	0.0160
50	0.0104

by Emets et al. [19] and Szymanski [20]. The balance of the competing mass transfer and light attenuation effects leads to an optimal bubbling rate, 0.5 L/min in this study.

3.1.4. Influence of initial concentration of BPA

Fig. 5 shows the effect of initial concentration of BPA on the photodegradation rate of BPA. The quasi-exponential decay observed during the photodegradation (Fig. 5) indicates pseudo-first order kinetics, which is strongly dependent on the initial concentration of BPA. Table 6 shows the rate constants at different initial concentration of BPA. It can be seen that the rate constant decreased with increasing concentration.

Langmuir–Hinshelwood (L–H) is a common model used to describe the influence of the initial concentration of substrate on the photocatalytic degradation rate of organic compounds [21]. The L–H model assumes that once the saturation point is reached, no further adsorption can occur. It is also assumed that there is no competition from reaction byproducts for the active sites. The simplest representation of the L–H model for the rate of disappearance of BPA is given by:

$$r_o = -\frac{dC}{dt} = \frac{k_r K C_o}{1 + K C_o} \quad (2)$$

where r_o is the initial rate of disappearance ($\text{mg}/(\text{L min})$) of BPA and C_o (mg/L) is its initial concentration. K represents the pseudo-equilibrium constant related to monolayer adsorption and k_r reflects the limiting reaction rate at maximum coverage for the experimental conditions. A linear expression is obtained when inverse initial rate is plotted against inverse initial concentration.

$$\frac{1}{r_o} = \frac{1}{k_r} + \frac{1}{k_r K} \times \frac{1}{C_o} \quad (3)$$

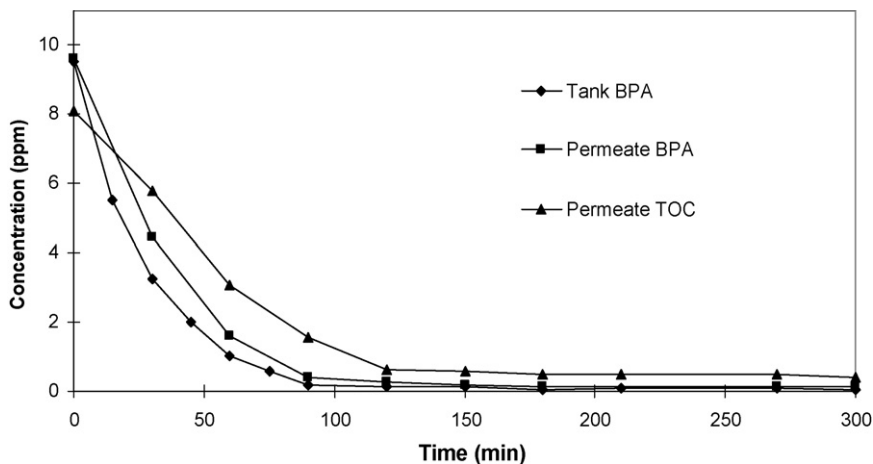


Fig. 6. Degradation and mineralization ratio of 10 ppm of BPA concentration (TiO_2 concentration = 0.5 g/L, initial pH 4, BPA feed concentration = 10 ppm, 0.5 L/min aeration rate).

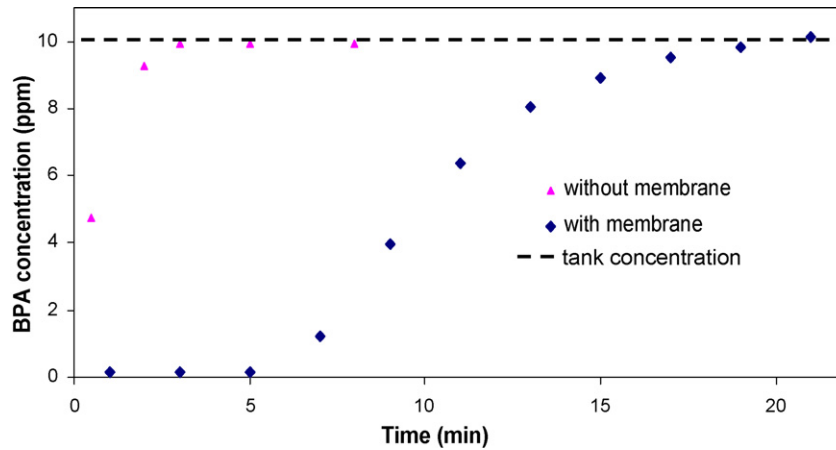


Fig. 7. Pulse tracer test for determination of permeate delay caused by adsorption of BPA on PVDF membrane (flux $100 \text{ L}/(\text{m}^2 \text{ h})$).

The kinetics of the different concentrations of BPA in the range of 5–50 ppm fitted well to the L–H model ($R^2 = 0.983$) giving $k_r = 0.476 \text{ mg}/(\text{L min})$ and $K = 0.044 \text{ L}/\text{mg}$. The Langmuir–Hinshelwood model has also been used extensively to describe the degradation of Auramine O [22] and phenol [3]. This type of reaction kinetics suggests that adsorption plays a key role in the photocatalytic degradation mechanism.

3.2. Degradation of BPA in submerged membrane photocatalytic reactor

Fig. 6 shows the degradation and mineralization efficiencies of BPA using the continuous SMPR. The pH, TiO_2 concentration and aeration rate were fixed at values of 4, 0.5 g/L and 0.5 L/min, respectively, in this series of experiments. A difference between the initial values of BPA and TOC was due to the fact that 79% by weight of BPA was organic carbon, i.e. 10 ppm BPA consists of 7.9 ppm of TOC (Eq. (1)). The permeate flux of Fig. 6 was kept at $100 \text{ L}/(\text{m}^2 \text{ h})$ which was equivalent to a BPA residence time of 2 h. This flux was chosen based on 95% mineralization of 10 ppm of BPA (1.5 h) in the batch degradation study.

From determination of the permeate quality by turbidity and particle size distribution measurements, the PVDF-MF membrane was found to be able to retain all TiO_2 particles. The concentration of BPA was reduced by 97% after 90 min of illumination and remained at this value until the end of the experiment (Fig. 6). It was observed that the permeate and the bulk concentration in the tank during the continuous photocatalysis process were different at the initial stage. The permeate BPA concentration was always higher than the bulk concentration until about 90 min. This could be due to adsorption/desorption of BPA on the membrane [23].

Separate pulse input tracer tests using BPA were conducted to confirm the possible adsorption of BPA on the membrane (Fig. 7). Without the presence of membrane, BPA took about 2 min to reach the same concentration as the tank value. The 2 min delay was calculated, using the permeate flow rate ($6.7 \text{ mL}/\text{min}$) and permeate dead volume (13 mL), to be the time necessary for BPA to travel from the tank to the end of the sampling tube. However, when the membrane module was added, it took about 22 min for BPA to reach the tank concentration which indicates that the 10 ppm BPA bulk in the tank took about 20 min to adsorb and saturate the membrane surface

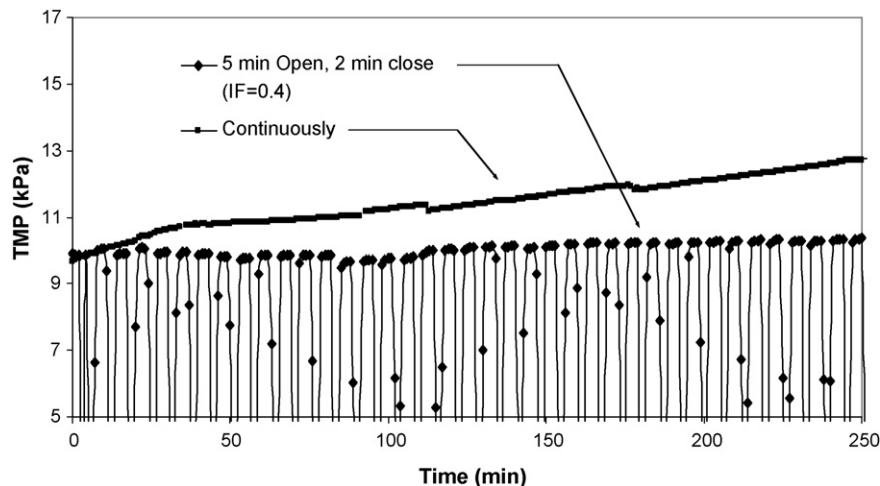


Fig. 8. TMP change for continuous $100 \text{ L}/(\text{m}^2 \text{ h})$ and intermittent permeation operation (intermittency of 2 min close/5 min open).

and the pores. These tests verified BPA adsorption on the PVDF membrane.

Before the start of any photocatalytic reaction, the continuous system was operated for 1 h in the dark so as to ensure that the system was in a steady state (inlet = tank = outlet BPA concentration). During this period of time, BPA would have been adsorbed on either the membrane surface or the membrane pores. When the UV lights were switched on, BPA concentrations in the bulk decreased continuously. BPA already adsorbed would be released and eluted when the lower concentration bulk solution permeated through the membrane thus resulting in higher permeate concentration as observed in Fig. 6. The discrepancy between the tank and permeate concentration ceased when the CSTR reaction reached a steady state at about 90 min.

One of the potential advantages of applying photocatalysis for the decontamination of water is the ability of this process to photomineralize all organic components, including target substrates and any intermediates formed. The destruction of intermediates is critical since some of the intermediates generated during the degradation of BPA could be more toxic than the parent compound, especially at low pHs [14]. At 60 min of Fig. 6, the concentration of TOC was about 3 ppm while the concentration of BPA was about 1.6 ppm, equivalent to TOC of 1.26 ppm. The difference between the concentration of TOC and BPA concentrations indicates the presence of intermediates during the PCO reaction. The SMPR process achieved 97% removal of BPA and 93% removal of all TOC at steady state.

Although a flux of 100 L/(m² h) in the SMPR allowed a high and continuous removal of BPA, some fouling of the membrane was observed at this flux. The TMP of the membrane steadily increased over the experiment to about 12.5 kPa from the initial 10 kPa as shown in Fig. 8.

There are several ways to alleviate fouling, for example by lowering the imposed flux or increasing aeration. However, increasing aeration would result in higher energy consumption and could also attenuate UV transmission as discussed earlier. Therefore, in order to maintain the high flux operation at low aeration rate, the effect of intermittent permeation was investigated

and the results are shown in Fig. 8. In this case, the permeation was closed for 2 min for every 5 min open. The choice of 2 min closed and 5 min open was arbitrary and further optimization is planned. When suction was stopped and no permeate was collected, there was a period for the aeration to exert shear on the membrane surface to facilitate the detachment of TiO₂ particles. This prevented an accumulation of TiO₂ particles on the membrane. The advantages of intermittent permeation to control fouling have also been reported by Howell et al. [10] and Hong et al. [24] during the operation of submerged membrane systems.

The intermittence frequency (IF) is defined as the ratio of the off time to on time. From a practical point of view, a lower IF would mean a higher production of purified water. Although the intermittent operation of 2 min off and 5 min on was shown to reduce the fouling tendency of the membrane as indicated in Fig. 8, it resulted in a decrease in water production by about 30% (Fig. 9, IF = 0.4). Therefore, an experiment with IF of 0.1 (1 min close, 10 min open) was carried out.

It is worth noting that the TOC mineralization with an IF of 0.1 was similar to that obtained with an IF of 0.4 and with continuous operations, i.e. 97% BPA reduction at 250 min (Fig. 9). The water production rate with IF of 0.4 and 0.1 are approximately 70 and 90% with respect to continuous production rate. Reducing the intermittence frequency from 0.4 to 0.1 has increased the water production rate by about 20%. Most importantly, it was found that the TMP of the system was decreased by five-fold with an IF of 0.1 compared to the continuous operation. As transmembrane pressure is proportional to the filtration energy cost [25], intermittent operation would reduce the operating cost of the continuous SMPR.

3.3. Importance of residence time

Filtration flux in a membrane separation–reaction process controls the mean residence time of the organic substrate in the system (assuming the membrane has zero retention of substrate). Control of residence time enables good degradation efficiency

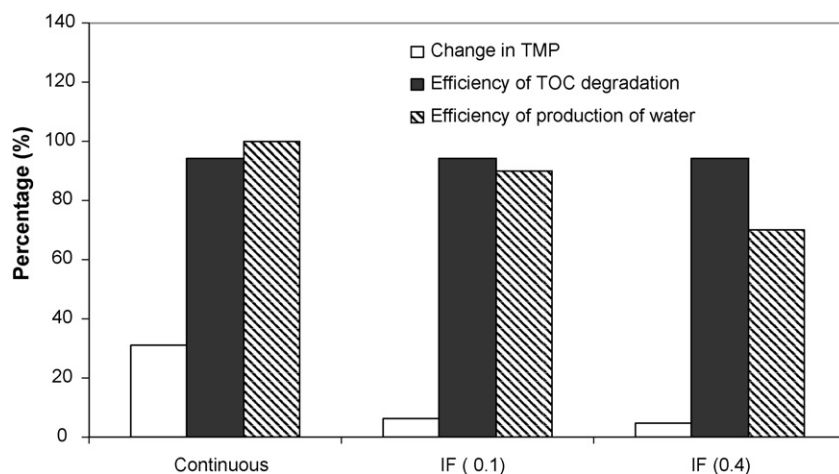


Fig. 9. Comparison of the TMP change, TOC degradation and production of water between continuous and intermittent permeation operation. [Change in TMP (%) = 100 × (initial TMP – final TMP)/initial TMP; efficiency of TOC degradation (%) = 100 × (initial TOC – final TOC)/initial TOC; efficiency of production of water (%) = 100 × volume of water at the designated flux/volume of water at 100 L/(m² h).]

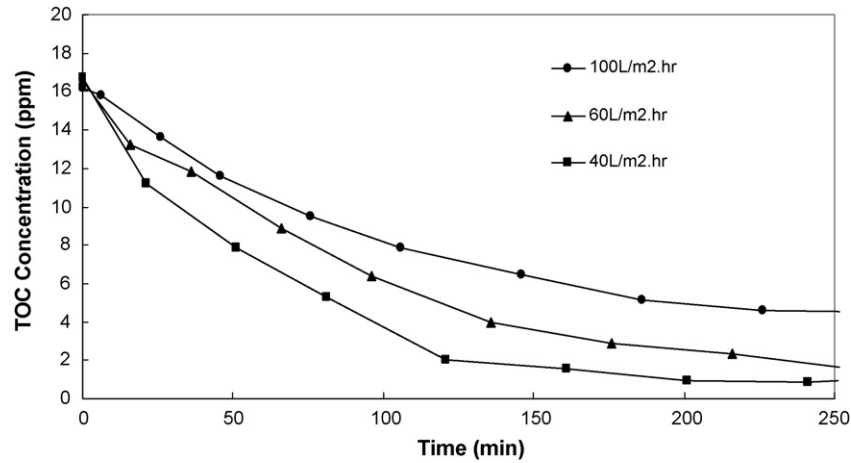


Fig. 10. Mineralization efficiency of 20 ppm of BPA by different permeate flux (TiO_2 concentration = 0.5 g/L, initial pH 4, BPA feed concentration = 20 ppm, 0.5 L/min aeration rate).

Table 7

Experimental conditions with different filtration fluxes (TiO_2 concentration = 0.5 g/L, initial pH 4, initial BPA concentration = 20 ppm, aeration rate = 0.5 L/min)

Filtration flux ($\text{L}/(\text{m}^2 \text{ h})$)	Residence time (h)
40	4.87
60	3.25
100	1.95

for higher concentration of organic substrate. Table 7 shows the relationship of filtration flux with residence time and the concentration of organic matter in the permeate. It is shown in Fig. 10 that longer retention times, i.e. slower permeate flux, resulted in better TOC removal efficiency. This was because the longer residence time had allowed more contacts between BPA and TiO_2 for oxidation to take place in the SMPR. A flux of $60 \text{ L}/(\text{m}^2 \text{ h})$ was deemed a better choice for achieving high removal rate (90%) of 20 ppm of BPA.

As expected, the lower filtration flux also led to less TMP rise (Fig. 11). When the flux rate was maintained at 40 or $60 \text{ L}/(\text{m}^2 \text{ h})$,

the amount of TiO_2 particles retained on the membrane surface per unit time was lower than that seen at $100 \text{ L}/(\text{m}^2 \text{ h})$. In addition, the applied aeration rate of 0.5 L/min was able to exert adequate shear rate on the vicinity of the membrane and to facilitate the detachment of any TiO_2 particles from the membrane surface at lower permeate fluxes thus resulting in smaller TMP changes.

3.4. Pseudo-first order model analysis of SMPR

The RTD determined in the sodium chloride test is presented in Fig. 12. As shown, the observed mean residence time (37.5 min) was very similar to the expected residence time of 40 min [$t = \text{volume of reactor}/(\text{flux} \times \text{area})$]. This result verified the use of the CSTR concept. In this section, pseudo-first order reaction kinetics combined with the ideal CSTR model is applied to evaluate the effect of initial concentration of BPA on the performance of BPA. The design equation in an isothermal stirred tank reactor is [26]:

$$C_A - C_{Af} = -kC_A\vartheta \quad (4)$$

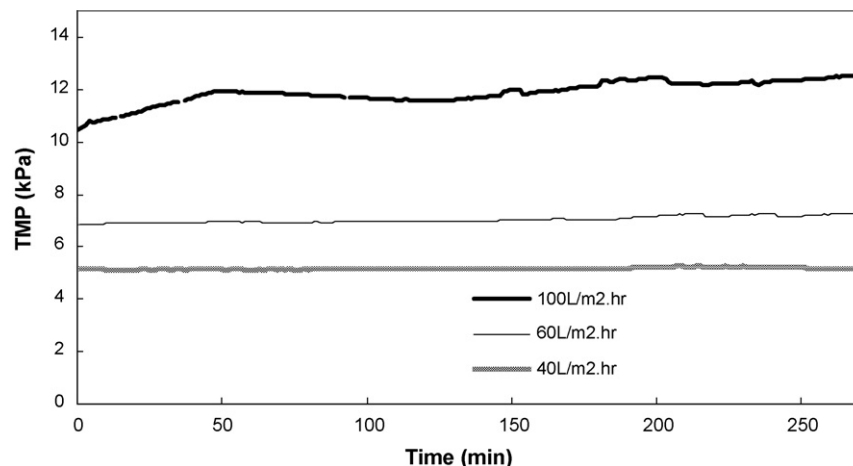


Fig. 11. Effect of different filtration flux on the TMP development (TiO_2 concentration = 0.5 g/L, initial pH 4, BPA feed concentration = 20 ppm, 0.5 L/min aeration rate).

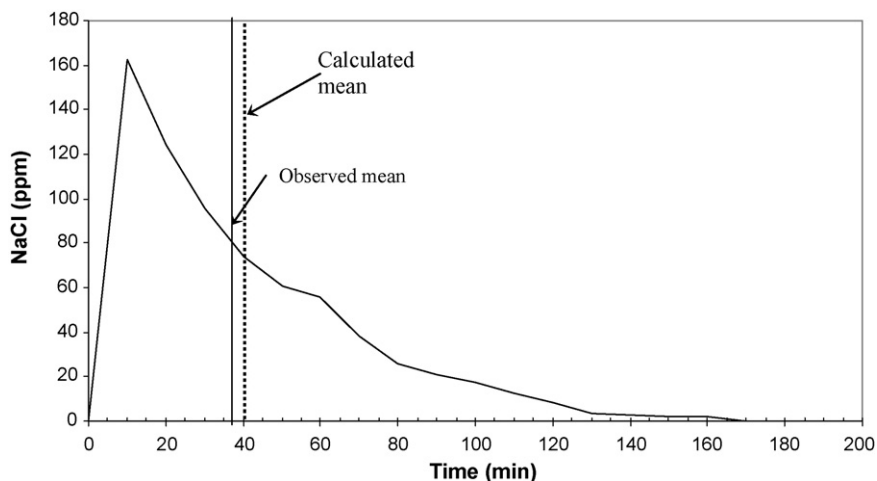


Fig. 12. Sodium chloride tracer experimental data for determination of hydraulic residence time distribution of the continuous SMPR.

by differentiation, we get

$$\frac{dC_A}{dt} = \frac{1}{\vartheta}(C_{Af} - C_A) - kC_A \quad (5)$$

where C_A is the substrate concentration at time t , C_{Af} the feed concentration and ϑ is the residence time of substrate. The analytical solution to Eq. (5) yields:

$$C_A(t) = C_{AO} e^{-(1/\vartheta+k)t} + \frac{C_{Af}}{1+k\vartheta} [1 - e^{-(1/\vartheta+k)t}] \quad (6)$$

By using the rate constants (Table 6) obtained from the batch experiments, the experimental data of the continuous SMPR permeate concentration was fitted as shown in Fig. 13. At the initial stage, the measured results for the 20 ppm test were higher than the predicted ones. This could be due to the desorption of BPA from the membrane surface or pores into the permeated bulk solution during the initial phase of the photocatalytic reaction whereby the concentration of bulk solution decreased rapidly. The desorption effect was less as the initial concentration of BPA got higher (30 and 50 ppm).

As discussed previously in the batch system study, the degradation rate of BPA depends strongly on the initial concentration of BPA. The discrepancies between the experimental data and the model observed during the steady-state experiments might thus be due to the concern that the model does not take into account the changes in the kinetic rate constants as the concentration of BPA changes in the continuous system. It was also suspected that the formation of a TiO_2 cake layer on the membrane surface (at $100 \text{ L}/(\text{m}^2 \text{ h})$) could have acted as a plug flow reactor (PFR) which might aid in the photodegradation of BPA. Sousa and Mendes [27] and Tsuru et al. [28] have modeled TiO_2 catalytic membrane systems as a PFR. The latter reported an enhanced performance of the photocatalytic reaction system with membrane organics permeating through a layer of TiO_2 . Thus, in order to overcome the limitations of the simple CSTR analysis, further model development is underway which takes into account the changing kinetic rate constants and the adsorption/desorption organics on the membrane itself and will be reported in a future publication.

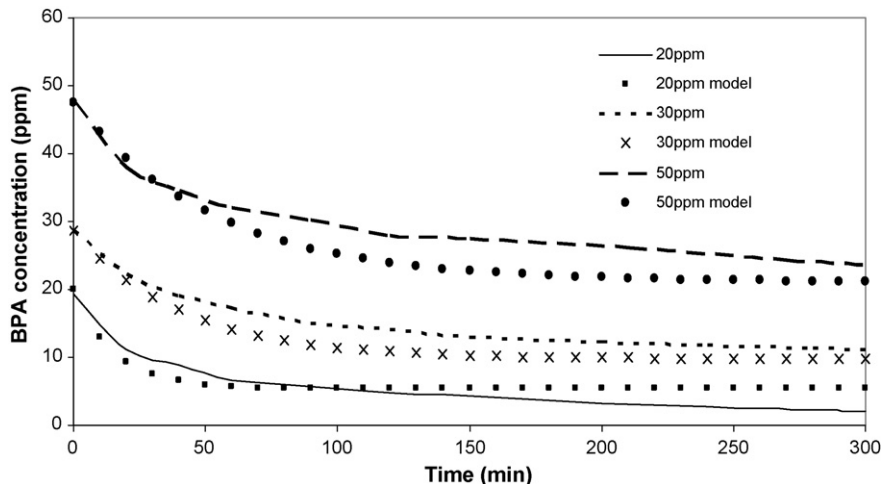


Fig. 13. Kinetics of BPA photodegradation with preliminary model fitting (flux = $100 \text{ L}/(\text{m}^2 \text{ h})$).

4. Conclusions

The current work has examined the factors affecting the performance of a SMPR. The photocatalysis process was first optimized before combining the membrane separation with the degradation process. pH was found to affect the degradation of BPA most significantly compared to effect of TiO₂ concentration and aeration rate. Lowering pH enhanced the degradation of BPA due to better adsorption on the catalyst. Increasing aeration rate, up to 0.5 L/min, increased the photocatalytic efficiency which then declined at higher aeration rate. The limit to the enhancing effect of the aeration was most probably due to the competing effects between the enhancement of mass transfer and light attenuation by bubble clouds which were formed at high aeration rate. The continuous SMPR was able to photodegrade 97% of the BPA and photomineralize 93% of the TOC after 90 and 120 min of UV illumination, respectively. The current work has also demonstrated the possibility of operating the SMPR at a high flux (100 L/(m² h)) with low membrane fouling using an intermittent permeation method. The importance of residence time control in the SMPR by varying the permeate filtration flux was demonstrated. An attempt to fit the basic CSTR model had only limited success. Discrepancies are attributed to the effect of adsorption/desorption of organics on the membrane and also the changing rate constants with organic concentration. For an efficient SMPR, factors influencing both photocatalytic degradation and membrane filtration, including fouling control, have to be taken into consideration.

Acknowledgement

The authors would like to acknowledge financial support from ASTAR (Singapore) as part of the Temasek Professorship Programme on Membrane Technology for Sustainable Water.

References

- [1] D.S. Bhatkande, V.G. Pangarkar, A. Beenackers, Photocatalytic degradation for environmental applications—a review, *J. Chem. Technol. Biotechnol.* 77 (2001) 102–111.
- [2] M. Butterfield, P.A. Christensen, T.P. Curtis, J. Gunlazaurd, Water disinfection using an immobilized titanium dioxide film in a photochemical reactor with electric field enhancement, *Water Res.* 31 (1997) 675–677.
- [3] A. Sobczynski, L. Duczmal, W. Zmudzinski, Phenol destruction by photocatalysis on TiO₂: an attempt to solve the reaction mechanism, *J. Mol. Catal. A: Gen.* 213 (2) (2004) 225–230.
- [4] P. Fernandez-Ibanez, J. Blanco, S. Malato, F.J. Nieves, Application of the colloidal stability of TiO₂ particles for recovery and reuse in solar photocatalysis, *Water Res.* 37 (2003) 3180–3188.
- [5] D. Beydoun, R. Amal, G. Low, S. McEnvoy, Novel photocatalyst: titanium coated magnetic-activity and photodissolution, *J. Phys. Chem. B* 104 (18) (2000) 4387–4396.
- [6] R. Molinari, M. Borgese, E. Drioli, L. Palmisano, M. Schiavello, Hybrid processes coupling photocatalysis and membranes for degradation of organic pollutants in water, *Catal. Today* 75 (2002) 77–85.
- [7] R. Molinari, L. Palmisano, E. Drioli, M. Schiavello, Studies on various reactor configurations for coupling photocatalysis and membrane processes in water purification, *J. Membr. Sci.* 206 (2002) 399–415.
- [8] D.D. Sun, J.H. Tay, K.M. Tan, Photocatalytic degradation of *E. coliform* in water, *Water Res.* 37 (14) (2003) 3452–3462.
- [9] A.G. Fane, S. Chang, E. Chardon, Submerged hollow fibre membrane module—design options and operational considerations, *Desalination* 146 (2002) 231–236.
- [10] J.A. Howell, H.C. Chua, T.C. Arnot, In situ manipulation of critical flux in a submerged membrane bioreactor using variable aeration rates, and effects of membrane history, *J. Membr. Sci.* 242 (2004) 13–19.
- [11] J. Fu, M. Ji, L. Jin, Submerged membrane photocatalysis reactor for fulvic acid removal in drinking water by using nanoparticle TiO₂, in: *Proceedings of the 3rd IWA Leading-Edge Conference and Exhibition on Water and Wastewater Treatment Technologies*, Sapporo, Japan, June 6–8, 2005.
- [12] S.S. Chin, K. Chiang, A.G. Fane, The stability of polymeric membranes in a TiO₂ photocatalysis process, *J. Membr. Sci.*, in press.
- [13] N. Watanabe, S. Horikoshi, H. Kawabe, Y. Sugie, J. Zhao, H. Hidaka, Photodegradation mechanism for Bisphenol A at the TiO₂/H₂O interfaces, *Chemosphere* 52 (2003) 851–859.
- [14] K. Chiang, T.M. Lim, L. Tsen, C.C. Lee, Photocatalytic degradation and mineralization of bisphenol A by TiO₂ and platinumized TiO₂, *Appl. Catal. A: Gen.* 261 (2) (2004) 225–237.
- [15] C.C. Wong, W. Chu, The direct photolysis and photocatalytic degradation of alcohol at different TiO₂ and UV sources, *Chemosphere* 50 (2003) 981–987.
- [16] J.H. Lee, W. Nam, M. Kang, G.Y. Han, K.J. Yoon, M.-S. Kim, K. Ogino, S. Miyata, S.-J. Choung, Design of two types of fluidized photo reactors and their photo-catalytic performances for degradation of methyl orange, *Appl. Catal. A: Gen.* 244 (1) (2003) 49–57.
- [17] K. Soparajee, S.A. Qasim, S. Basak, K. Rajeshwar, An integrated flow reactor-membrane filtration system for heterogeneous photocatalysis. Part II: experiments on the ultrafiltration unit and combined operation, *J. Appl. Electrochem.* 29 (1999) 1111–1118.
- [18] Y. Jia, R. Wang, A.G. Fane, Atrazine adsorption in water by powdered activated carbon-improved mass transfer by bubbling, *Chem. Eng. J.*, in press.
- [19] E.P. Emets, G.Yu. Kolomeyts, P.P. Polluektov, V.V. Timonin, Control of disactivation processes by using a new laser bubble sizer, *J. Aerosol Sci.* 27 (Suppl. 1) (1996) S559–S560.
- [20] W.W. Szymanski, Optical behaviour of fine bubbles—possibility of real time size characterization, *J. Aerosol Sci.* (Suppl. 1) (1996) S537–S538.
- [21] J. Cunningham, G. Al-Sayyed, S. Srijaranai, Adsorption of model pollutants onto TiO₂ particles in relation to photoremediation of contaminated water, in: G. Helz, R. Zepp, D. Crosby (Eds.), *Aquatic and Surface Photodemists*, Lewis Publishers, CRC Press, 1994, pp. 317–348.
- [22] I. Poullos, A. Avrana, E. Rekliti, A. Zouboulis, Photocatalytic oxidation of Auramine O in the presence of semiconducting oxides, *J. Chem. Technol. Biotechnol.* 75 (2000) 205–212.
- [23] J.-S. Kim, S.-J. Lee, S.-H. Yoon, C.-H. Lee, Competitive adsorption of trace organics on membranes and powdered activated carbon in powdered activated carbon-ultrafiltration system, *Water Sci. Technol.* 34 (9) (1996) 223–229.
- [24] S.P. Hong, T.H. Bae, T.M. Tak, S. Hong, A. Randall, Fouling control in activated sludge submerged hollow fiber membrane bioreactors, *Desalination* 143 (3) (2002) 219–228.
- [25] M. Cheryan, *Ultrafiltration and Microfiltration Handbook*, Technomic, Lancaster, PA, 1998.
- [26] O. Levenspiel, *Chemical Reaction Engineering*, third ed., John Wiley and Sons Inc., New York, 1999.
- [27] J.M. Sousa, A. Mendes, Modeling a dense polymeric catalytic membrane reactor with plug flow pattern, *Catal. Today* 82 (2003) 241–254.
- [28] T. Tsuru, T. Kan-No, T. Yoshioka, M. Asaeda, A photocatalytic membrane reactor for gas-phase reactions using porous titanium dioxide membranes, *Catal. Today* 82 (2003) 41–48.